Journal of Intelligent Manufacturing
https://doi.org/10.1007/s10845-023-02277-z

Post-processing of powder bed fused stainless steel: micro-machining and micro-electrical discharge machining

Andrea Abeni[1] · **Mariangela Quarto**[2] · **Paola Serena Ginestra**[1]

Received: 19 July 2023 / Accepted: 10 November 2023

Abstract
Surface quality is often a specific requirement when dealing with Additive Manufacturing and dimensional accuracy, especially during 3D printing of metals. Therefore, it is crucial to evaluate the material removal behavior of Powder Bed Fusion specimens during Micro-Mechanical Machining and Micro-Electrical Discharge Machining procedures to detect their machinability responses. In this paper, micro-machining of 17-4PH stainless steel samples produced by Laser Powder Bed Fusion is reported. Specifically, we performed Micro-Mechanical Machining and Micro-Electrical Discharge Machining operations, analysed the process performances, and compared the machining conditions. Additionally, we investigated the surface roughness and burrs extension as a function of geometrical configuration and process parameters. The outcomes of this work regard the processing conditions and parameters to optimize the machining operations on 3D-printed metal samples. This work allows the identification of specific features resulting from each process in relation to the material removal rate, giving the possibility to compare and evaluate the machining conditions for 3D parts post-processing.

Keywords Powder Bed Fusion · Micro-machining · Micro electrical discharge machining

Introduction

Powder Bed Fusion (PBF) technologies produce metal parts with different properties (e.g., density, surface quality, mechanical performances, etc.) in comparison with conventional manufacturing techniques (Kasperovich et al., 2016; Korner C & Group F, 2016). The Laser Powder Bed Fusion (LPBF) technique works with a focused laser beam that selectively melts metal powders, layer upon layer, in an enclosed chamber to obtain high-density and complex parts. The material behavior of a metal sample fabricated with LPBF is influenced by the alterations typical of the melting process on the final microstructure properties (Cooke et al., 2020; Tan et al., 2020). Furthermore, the surface integrity of 3D-printed metal samples is poor and with high variability causing important consequences on the mechanical properties (tensile and compressive strength, brittleness, fatigue strength, etc.) and compromising the suitability for the final applications (Bai et al., 2021; Galati et al., 2019; Liu et al., 2020). With a variety of approaches, including thermal treatments to improve microstructure, hot/cold isostatic pressing to reduce porosity, and subtractive processes to regulate surface and shape, many researchers have attempted to reduce the defects from 3D-printed metals. It has been investigated to process 3D-printed metals using both conventional subtractive techniques (such as turning, milling, and drilling) and unconventional subtractive techniques (such as laser polishing, electrochemical polishing, and abrasive flow machining). Traditional and non-traditional processes can be used for machining 3D-printed metals playing a significant role in post-processing operations to: restore geometrical accuracy and surface quality, complete 3D processes because 3D techniques cannot accurately generate precise details like

✉ Andrea Abeni
andrea.abeni@unibs.it

Mariangela Quarto
mariangela.quarto@unibg.it

Paola Serena Ginestra
paola.ginestra@unibs.it

[1] Department of Mechanical Engineering, University of Brescia, Via Branze 38, 25123 Brescia, BS, Italy

[2] Department of Management, Information and Production Engineering, University of Bergamo, Dalmine, BG, Italy

Published online: 21 December 2023

internal and external threads or features with tight form tolerance (e.g., flatness, cylindricity) and remove of supporting material.

Micro-manufacturing is becoming an interesting field of production and great effort is going towards the production of reduced-size and weight products for aerospace, automotive, and biomedical applications (Bissacco et al., 2008). These applications, combined with the introduction of newly developed and advanced materials with complex designs, have exploited the use of both conventional and unconventional machining processes. Conventional Micro-Mechanical Machining (MM) operations are widely used to change the surface integrity of parts and, among other conventional techniques, MM is preferable, especially when dealing with custom-made structures built layer by layer (Coz et al., 2020; Khaliq et al., 2020; Varghese & Mujumdar, 2021). MM is very convenient to obtain micro-size features on a wide variety of materials in terms of volume and cost ratio. The process works by mechanical material removal with a micro tool and a chip thickness that is comparable to the size of the cutting-edge radius of the mill. The relevant process parameters are the depth of cut (a_p), the cutting speed (v_c), and the feed per tooth (f_z). The combination of the process parameters allows computing the Material Removal Rate (*MRR*). The Minimum Uncut Chip Thickness (MUCT) must be first calculated to identify the ploughing regime during cutting (Abeni et al., 2022; Sahoo et al., 2020). Considering the non-conventional processes, Micro-Electrical Discharge Machining (micro-EDM) is mostly used with difficult-to-cut materials (D'Urso et al., 2020; Kumar et al., 2020) to realize microchannels and micro-holes with high aspect ratios. The material removal during micro-EDM occurs by the thermal energy developed by electrical discharges generated in a gap between the electrode and the workpiece that are not in contact with each other but in a dielectric fluid. The most significant parameters for the micro-EDM process are peak current, voltage, pulse width and frequency, and their combinations which define the average *MRR*.

Due to the complexity of both considered processes, it is usually difficult to predict the process performances (machining time, geometrical deviation, tool wear, etc.). Thus, process optimization as a function of part miniaturization, dimensional precision, and part quality is a complex aspect. Since different micro-scale features can be alternatively produced with MM or micro-EDM, a proper analysis of each process outcome on 3D-printed parts is crucial to assess the optimal machining operation for a specific application.

Researchers have recognized the possibility to use micro-machining methods as post-processing on AM products (Coz et al., 2017; Greco et al., 2021; Karakılınç et al., 2023; Nas & Akıncıoğlu, 2019). Due of the inhomogeneous characteristics of a 3D workpiece, it is more difficult to machine materials from LPBF than from wrought materials of the same composition (Franczyk et al., 2021 Jan 15). Micro-scale machining presents more difficulties than conventional machining because the former is more sensitive to microstructure changes as a result of 3D process parameters and variable cooling rates at various spots on a 3D-printed product. However, the machinability of 3D-printed metals is different from the wrought metals obtained by conventional methods. Therefore, researchers have investigated the micro-machining of 3D-printed alloys such as Ti–6Al–4V, 316L stainless steel, and others (Gomes et al., 2022). On the other hand, non-traditional micro-machining has been rarely investigated for the processing of PBF parts (Hassanin et al., 2016). Moreover, micro-machining process optimization on PBF parts is not always reported, especially when investigating traditional and non-traditional processes together.

For these reasons, this study aims to investigate the material removal behavior of 17-4PH stainless steel parts that have been produced by LPBF and post-processed using micro-EDM and MM. The objective of this work is to report useful information to validate the machining possibilities (in the micro scale) offered by traditional and non-traditional machining techniques leading to a more comprehensive understanding of the post-processing impact related to the process parameters. Specifically, the study focuses on the machining of specific features: microchannels with widths of 200 and 800 μm and micro-holes with diameters of 200 and 800 μm. Both sizes regard the micro-machining field, but 800 μm is close to the transition to conventional macro-machining and the results comparison can be useful to highlight the size effects. Also, in this work, the analysis is carried out on the dimensional accuracy of each process as a function of the *MRR*. Further, Surface roughness (Sa) and burrs dimensions were measured to relate the surface finishing to the material deformation mechanism during the processes.

Materials and methods

The comparison between MM and micro-EDM was performed on 17-4PH stainless steel samples fabricated by LPBF. The sample fabrication and the machining processes are described in the following sections. The comparison was carried out by manufacturing microchannels and micro-holes with two different sizes (200 μm and 800 μm) and by testing different levels of *MRR* for MM and micro-EDM. The features were produced on the as-built samples without performing any mechanical, chemical, or thermal treatments.

Table 1 Chemical composition of 17-4PH stainless steel powder

17-4PH	Fe	C	Cr	Ni	Cu	Mn	Mo	Nb	Si
Wt (%)	Bal	< 0.07	16.71	4.09	4.18	0.8	0.19	0.23	0.53

Table 2 Process parameters used in the LPBF process

Process Parameter	Value
Laser power (W)	50
Spot diameter (μm)	80
Scan speed (mm/s)	300
Hatch spacing (μm)	50
Layer thickness (μm)	30

Additive manufacturing

The samples were designed as parallelepipeds with a square base of 25 × 25 mm and a height of 2.2 mm. Four holes, each with a diameter of 4.20 mm, were included at the corners to securely constrain the samples on the machine frame. The samples were fabricated using the commercial LPBF machine ProX 100 (3D System, Rock Hill, USA) in a Nitrogen atmosphere with a controlled O_2 content lower than 0.1 vol% to avoid impurities. Table 1 reports the chemical composition of the 17-4PH stainless steel powder used as printing material, while Table 2 summarizes the applied printing parameters.

Samples pre-processing

For the machining tests, two identical samples were fabricated with the same geometry. One sample was used for performing the MM features, while the second one was machined by micro-EDM to replicate the features, such as microchannels and micro-holes, illustrated in Fig. 1. Each feature was machined with three different *MRRs* and each test was repeated three times to ensure statistical validity of the analysis.

The holes with two different sizes (diameter 200 μm (Fig. 1a) and 800 μm (Fig. 1b)) were fabricated on the top surface. Since the sample height was 2.2 mm, a pocket with a depth of 1.2 mm was previously fabricated by machining the bottom surface of both samples to micro-machine holes with a depth equal to 1 mm (Fig. 1c). The channels were machined on four pockets, each with a depth of 0.2 mm on the top surface of both samples. The planar surfaces were rough-machined using a four-flute flat-bottom end mill with a nominal diameter of 3 mm. The cutting speed was set equal to 80 m/min while the feed per tooth was set equal to 5 μm/tooth. To ensure the workability of the channels during the MM and micro-EDM processes, it was decided to flatten the surface for the creation of the channels. Preliminary tests showed that the high roughness and the low planarity of the as-built surface caused difficulties in machining due to the variability of the actual depth of cut of the microchannels.

The channels were machined in a single pass and had two different sizes, 200 μm and 800 μm in width, with a constant length of 5 mm. The depth of the channels was 20 μm for the channels with a width of 200 μm (Fig. 1d) and 50 μm for the channels with a width of 800 μm (Fig. 1e).

Micro-machining

The MM tests were performed on the ultra-precision five-axis nano-precision machining center KERN Pyramid Nano (Kern Micro Technik, Olympiastr. 2, D-82418 Murnau-Westried Germany) with a spindle able to reach 45,000 RPM, equipped with a Heidenhain iTCN 530 numeric control.

The microfeatures were machined by using standard tungsten carbide tools with titanium nitride coating, as listed in Table 3. The micro-mill is an integral flat-bottom-end mill.

The drilling tests were performed by implementing a tap-drilling strategy to remove the metal chip correctly. The channels were machined by moving the tool from the outer to the center of the sample at a constant depth single pass. The tools paths were defined through commercial CAM software Solidworks ® CAM and the Minimum Quantity Lubrication (MQL) with a non-water-soluble, high-performance lubricant (UNILUBE 9107), was used. The MQL system of KERN Pyramid Nano allows to control the airflow and the quantity of oil particles inside the stream. The regulation is manageable through a modulating valve and previous tests allowed to find a tradeoff between the necessity of lubrication in the working area and the evacuation of the oil from the workpiece. The MQL fluid is injected through a nozzle manually oriented in the area of contact between the sample and the tool. The process parameters used in this study were based on the results of a previous process characterization (Abeni et al., 2021a). The feed per tooth was kept constant for all the experiments. On the contrary, the cutting speed was varied on three levels, as listed in Table 4, to evaluate how it influences micro-machinability, in terms of features dimensions and variability, burr size, and surface roughness. The *MRR* was computed to compare the productivity of micro-machining with micro-EDM. It was calculated as the product of the feed rate and the section of the machined channels and

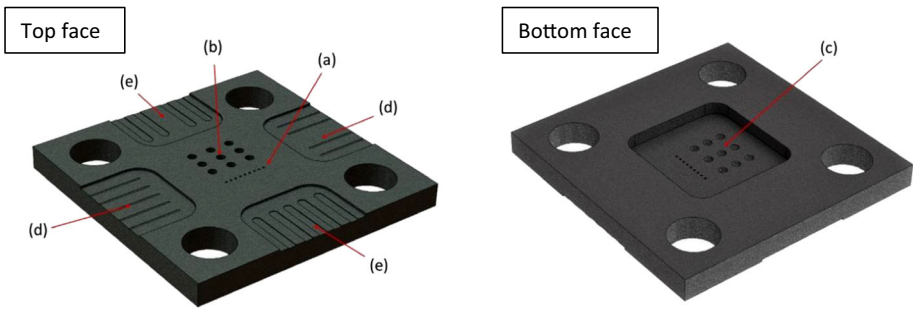

Fig. 1 Render of the machined samples, the top surface on the left and the bottom surface on the right. (a) holes with a diameter of 200 μm, (b) holes with a diameter of 800 μm, **c** pocket with a depth of 1.2 mm, (d) channels with a width of 200 μm, (e) channels with a width of 800 μm

Table 3 List of micro-tools utilized in micro-machining

Code	Rime HM79/08	Rime HM79/02	Mitsubishi MSE0080B	Mitsubishi MSE0020B
Type	Micro-mill	Micro-mill	Micro-drill	Micro-drill
Nominal diameter (μm)	800	200	800	200
Number of tool flutes	2	2	2	2
Helix angle (°)	30°	30°	30°	35°
Material	Tungsten carbide	Tungsten carbide	Tungsten carbide	Tungsten carbide
Material coating	Titanium nitride	Titanium nitride	Titanium nitride	Titanium nitride

Table 4 Process parameters used in the micro-machining process

Tool diameter (μm)	Cutting speed (m/min)	Depth of cut (only micro-milling) (μm)	Feed per tooth (μm/tooth)	*MRR* channels (mm^3/min)	*MRR* holes (mm^3/min)
200	18	20	1	0.23	1.80
	22	20	1	0.28	2.20
	26	20	1	0.33	2.60
800	30	50	3	2.86	36.0
	40	50	3	3.82	48.0
	50	50	3	4.77	60.0

holes, and is reported in Table 4. The tool wear was measured with a digital optical microscope and was found to be negligible.

Micro-EDM

The printed samples were worked on a Sarix SX-200 (Sarix SA, Sant'Antonino, CH) micro-EDM, and a CAM software was used to define the electrode paths for the generation of the micro-features. Two cylindrical tungsten carbide electrodes were tested considering 200 μm and 800 μm diameters. Hydrocarbon oil was used as a dielectric medium. For each electrode, three electrical discharge shapes were tested: short, medium, and long pulses. The shape of the electrical pulses used in the micro-EDM process differs in terms of the current peak and width. These parameters, in relation to the electrode, workpiece materials, and geometry, determine the average value of the material removal rate (*MRR*).

Table 5 reports the average value of the material removal rate (*MRR*) defined for the experiments. The values were derived from the evaluation of preliminary tests that were necessary to identify the optimal combination of process parameters. This combination was selected to reduce the probability of short circuits and ensure process stability and repeatability. The machine generates reports containing information about the performed process, including the estimated material removal rate (*MRR*) as the ratio between the removed volume and the machining time. Using the CAM software, it was possible to set the average value of the *MRR*. The results were then evaluated by comparing them to those obtained with different *MRR* values. It is important to note that on this machine, the peak current cannot be defined in terms of its actual intensity (amperes). Therefore,

Table 5 Process parameters used in micro-EDM process

Electrode diameter (μm)	Pulse shape	Average *MRR* (mm^3/min)	Peak current (index)	Voltage (V)	Width (μs)
200	Short	0.00021	100	90	2
	Medium	0.00169	100	100	4
	Long	0.00668	100	100	5
800	Short	0.00787	100	90	2
	Medium	0.01074	100	100	4
	Long	0.10820	100	100	5

the reported values are presented as an index. It is important to note that this index cannot be directly translated into a current intensity, as the peak value can vary depending on factors such as pulse shape and duration. While the analysis of electrical discharges is not the main focus of this study, previous research (Quarto et al., 2019) has shown that peak currents typically range between 4A (for short pulses) and 29A (for long pulses).

Burrs and recast particles evaluation

MM and micro-EDM fundamentals are different and the resulting characteristics of the machined parts, which affect the quality of the final product and the desired functionality, are not the same. Considering the differences between the two processes, it is possible to analyze the formation of burrs for MM and the presence of recast particles for the micro-EDM. The aim of this study is not to compare the effects of these phenomena on the final components but rather to provide a comprehensive understanding of the processing of AM parts by evaluating their contributions.

As previously mentioned, the MM process leaves burrs and accumulated materials on the boundaries of the machined features, which are proportional to the feed rate. When manufacturing channels using micro-EDM, the machining defects are represented by recast particles deposited on the channel surfaces. This issue is not present or is very limited in micro-EDM drilling. Therefore, two techniques were defined for evaluating burrs and recast particles.

A method was developed to quantify the extension of burrs using the Sensofar S-neox optical profilometer. The 3D topography measurement evaluates the projected area of the complex burr geometry, which is processed by the elaboration software. A 3D reconstruction of the surfaces of the channels and holes generates a points cloud containing the spatial distribution of the scanned points along x, y, and z directions. The form correction procedure is applied by performing a linear least-square fitting on the area related to the flat surface of the sample. A procedure to discriminate between the original surface of the part and the burrs was then conducted through the analysis of the z-height distribution defining a threshold value. This allowed us to estimate and approximate the extension of the burrs in terms of volume and projected area. An example of the applied method is reported in Fig. 2. It shows the evaluation of the burr for a hole (Fig. 2a) and a channel (Fig. 2b), respectively.

On the other hand, SEM high-resolution images acquired with backscattered electrons are utilized to evaluate the recast particles on the channels' bottom surfaces. These images were then elaborated through ImageJ image processing software (NIH, USA) to highlight the presence of recast particles and determine their extension in terms of percentage of area. Figure 3 shows the image elaboration process, demonstrating that the backscattering electrons differentiate the chemical elements based on their atomic weight. The white circular parts in Fig. 3a represent the recast particles, characterized by a chemical composition that is a mixture of the workpiece and electrode material. By defining a threshold based on the greyscale, the image elaboration software can isolate these particles and estimate their average dimensions and extension, as shown in Fig. 3b and c.

Dimensions and surfaces finishing

An autofocus laser probe equipment PF60 (Mitaka, JPN) was utilized to reconstruct the 3D geometry of the micro-features. After scanning, dimensional measurements were performed to evaluate the parameters and assess the impact of cutting speeds on the tolerances. The diameter and the circularity of each hole were measured, while the width of each channel was evaluated in two sections (distance of 1.25 mm and 3.75 mm from the sample edge) and each measurement was repeated three times to ensure accuracy. The surface finishing of the channel's bottom was analyzed by elaborating the raw data to obtain a surface description using the amplitude parameters defined by the international standard UNI EN ISO 25178:2019. For distinguishing between two profiles having the same S_a(Eq. 1), where $z(x, y)$ indicates the ordinate values defined in the area (A), two further amplitude parameters were considered: skewness (S_{sk}) and kurtosis (S_{ku}) (D'Urso et al., 2018). The surface skewness (Eq. 2) is

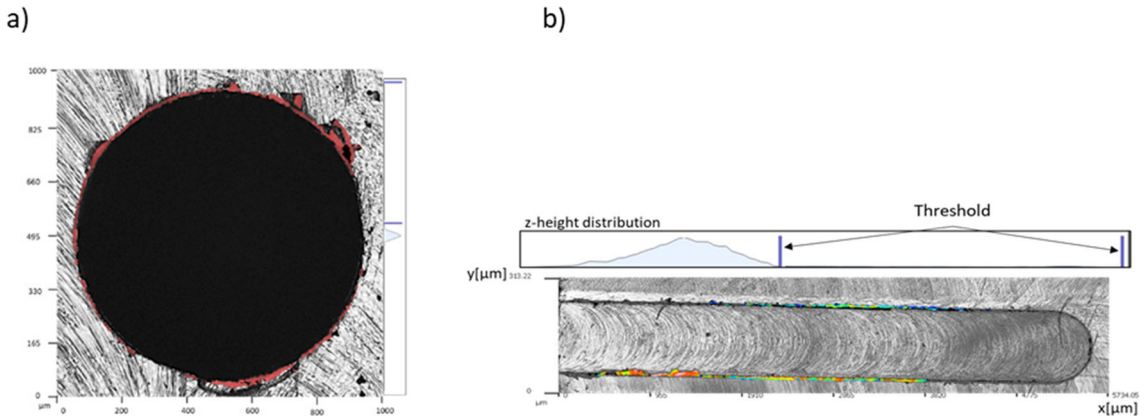

Fig. 2. 3D reconstruction overlapped by the burrs identification (coloured area) for holes (**a**) and channels (**b**) (Color figure online)

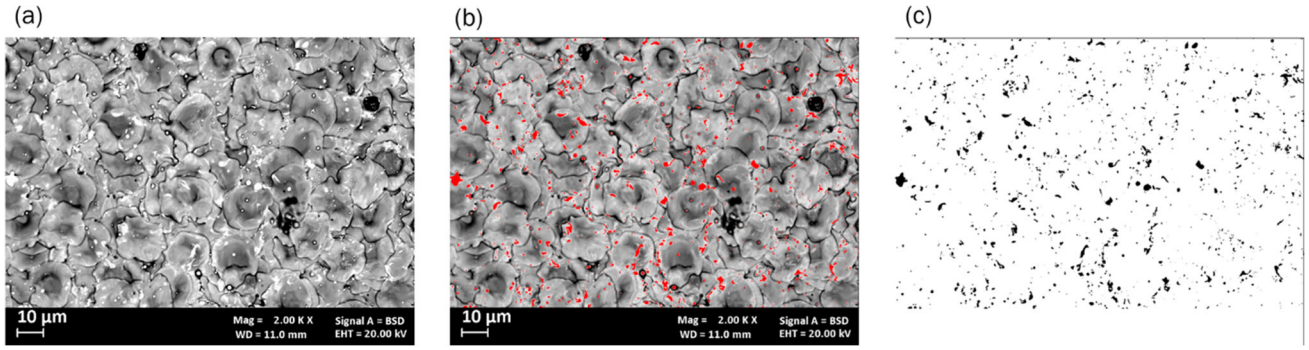

Fig. 3 Image elaboration process for estimation of recast particles. **a** Backscattering Sem image, **b** recast particles identification, **c** Recast particles evaluation

the third central moment of the profile amplitude probability density function, measured over the assessment length and quantifies how much the profile distribution deviates from a perfectly symmetrical distribution of the height profile. Perfectly symmetrical height distribution has zero skewness since the profile is characterized by as many peaks as valleys. It is calculated as the quotient of the mean cube value of the ordinate values and the cube of S_q within a defined area (A) The surface kurtosis (Eq. 3) is the fourth central moment of profile amplitude probability density function, measured over the assessment length and measures the sharpness of the probability density of the profile. It is calculated as the quotient of the mean quadratic value of the ordinate values and the fourth power of S_q within a defined area (A). If $S_{ku} < 3$ the distribution curve is said to be platykurtic and has relatively few high peaks and low valleys. On the contrary, if $S_{ku} > 3$, the distribution curve is said to be leptokurtic and has relatively many high peaks and low valleys (Shivanna et al., 2014).

$$S_a = \frac{1}{A}\iint_A |z(x,\ y)|dxdy \tag{1}$$

$$S_{sk} = \frac{1}{S_q^3}\frac{1}{A}\iint_A \left|z^3(x,\ y)\right|dxdy \tag{2}$$

$$S_{ku} = \frac{1}{S_q^4}\frac{1}{A}\iint_A \left|z^4(x,\ y)\right|dxdy \tag{3}$$

Results and discussion

Micro-drilling

During the drilling operation, the MM exhibits a strong limit. On the top surface of the as-built samples, micro-drilling of Ø 200 µm holes was not possible. The roughness of the as-built LPBF parts was tested on three replicates of the same samples and was equal to 12.85 ± 0.18 µm, causing significant tool bending and brittle failures regardless of cutting speed. Only after preliminary milling of the top surface to achieve a flat surface with a 3 mm flat-end mill at a depth of 50 µm, the Ø 200 µm holes were manufactured. The Ø 800 µm micro-drills also experienced considerable bending on the as-built surface but completed the realization of the micro-holes. The holes were drilled using the Ø 800 µm micro-drills.

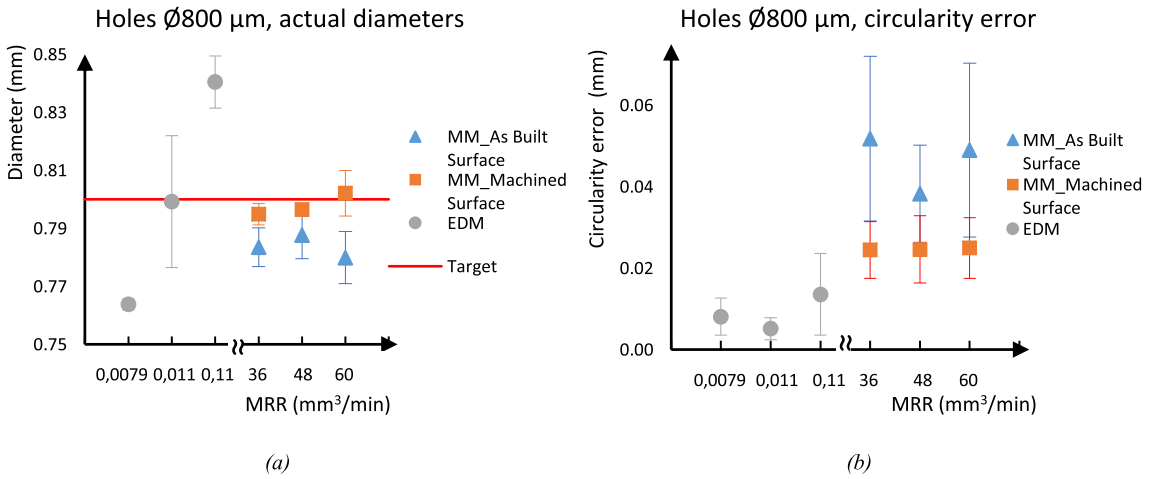

Fig. 4 Diameter (**a**) and circularity error (**b**) of the Ø 800 µm holes

The holes were again duplicated on the milled surface with the Ø 800 µm micro-drills to compare their actual diameter and circularity, as shown in Fig. 4. When compared to holes machined on the as-built surface, holes executed on the machined surface display higher accuracy, repeatability, and lower circularity error. More specifically, the holes drilled on the as-built surface were small and uneven in shape, potentially affecting mechanical coupling with other components. It is worthwhile to emphasize the material behavior on the planar surface. The diameter and circularity of the Ø 800 µm micro holes grow as the *MRR* increases, whereas the patterns are reversed for the Ø 200 µm micro-holes. The cutting speed v_c reported in Table 4 can be used to discuss one possible interpretation of this phenomenon: with the Ø 800 µm drill, a higher cutting speed can be achieved than with the Ø 200 µm drill due to the upper limit of the spindle speed. This might lead to poor cutting conditions due to material adherence to the tool. Cutting speeds with Ø 800 µm drills, on the other hand, are adequate, but the influence of tool run-out increases. The eccentricity of the drill rotation increases as the spindle speed increases, as does the diameter of the holes, however, the circularity remains constant and is unaffected by the cutting speed.

In both cases, drilling operations for micro-EDM were done on rough surfaces with no problems for the equipment. The data shown in Figs. 4a and 5a show no discernible patterns as a function of the *MRR*, neither for the diameters nor the circularity of the holes. For lower dimensions, it can be seen that micro-EDM delivers more repeatable outcomes. The effect is demonstrated by the low standard deviation of the observed diameters for the Ø 200 µm electrode. The difference of the resultant diameters from the goal value at the lowest and greatest *MRRs* is a notable observation for micro-EDM features. Electrode wear and secondary discharges cause this variance, which affects the precision of the hole diameters. The holes created with a Ø 200 µm electrode exhibited an under-sizing of the final features, which can be connected with a high amount of electrode wear, which reduces the diameter of the electrode, resulting in a "sharp" shape. In particular, because the measured surface has multiple peaks and valleys, the secondary discharge phenomena are increased when compared to machining on planar surfaces. This behavior appears to be different for the Ø 800 µm electrode, where the holes have substantial variability, increasing diameter. In this situation, the larger size of the electrode most likely generates an increase in the secondary discharges that impact the surface rather than removing material from the electrode as the Ø 200 µm electrode did. This effect can be reduced by machining on a prepared surface as shown for MM.

In general, based on the results shown in Figs. 4a and 5a, the average diameter of the micro-holes created by MM is closer to the target diameter due to the calibrated microdrills dimension and low tool run-out, particularly when drilling on a pre-prepared surface. The shape quality of the micro-machined holes, on the other hand, is lower than that of micro-EDM, as demonstrated by the larger circularity error values. Finally, the circularity error for MM holes increases with tool size, but it is unaffected by wire size in micro-EDM (Figs. 4b and 5b).

Microchannels

Figure 6 depicts the relationship between channel width and machining method as well as *MRR*. The low variability of channel width in both procedures implies strong repeatability and a small effect of the *MRR* on geometrical accuracy. This behavior may be connected to a reduction in secondary discharges due to less material around the electrode during

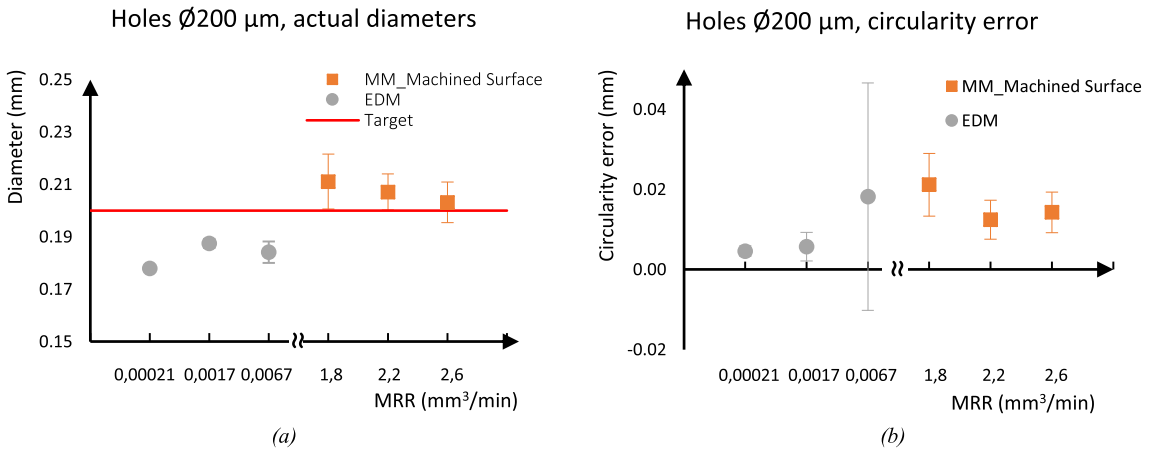

Fig. 5 Diameter (**a**) and circularity error (**b**) of the Ø 200 µm holes

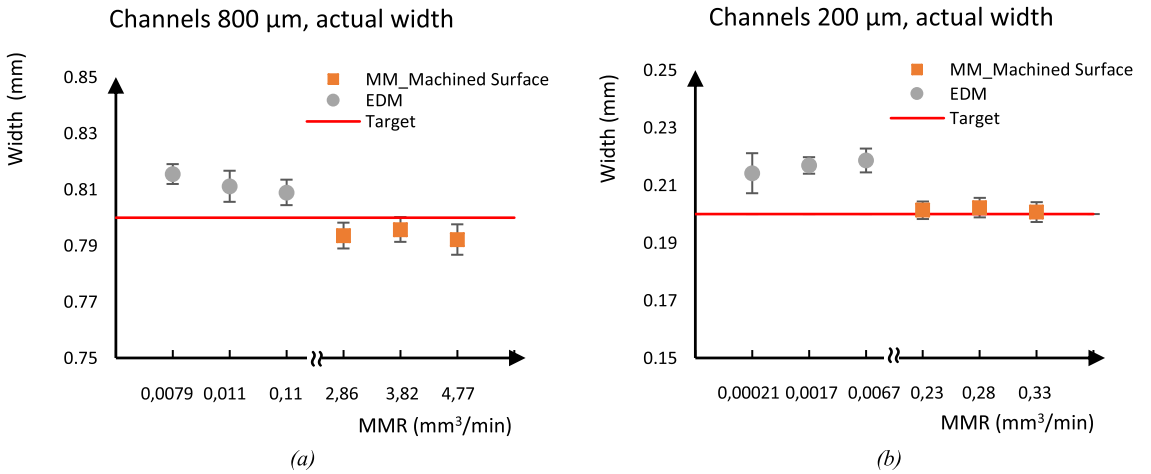

Fig. 6 Width of the channels with a nominal size of 800 µm (**a**) and 200 µm (**b**)

the machining process when compared to drilling for micro-EDM. Because secondary discharges are reduced, electrode wear is reduced, resulting in improved precision.

Figure 7 shows the surface finishing measurements at the bottom of the microchannels. It is clear how MM enabled improved surface finishing with a S_a smaller than 0.3 µm regardless of feature size or process settings. Micro-EDM S_a, on the other hand, is greater than 0.3 µm, with a maximum of 0.66 µm, due to the usual cratered surfaces. Using the 200 µm channels, it is feasible to see an increase in surface roughness as a function of *MRR*. The trends in 800 µm channels, on the other hand, are highly variable (Fig. 7b). These aspects can be related to the low effect of the *MRR* on the surface texture parameters since the discharge peaks and width are more effective as demonstrated in previous works (Abeni et al., 2021a).

About MM (Fig. 7a), the surface finishing of the channels with a width of 200 µm resulted worse than the finishing of the 800 µm channels in terms of absolute values and variability. An explanation is related to the chip formation mechanism considering the transition from shearing to ploughing phenomena (Abeni et al., 2021b; Balázs et al., 2021; Ji et al., 2021). When this happen, it is possible to observe the formation of a negative rake angle determining irregular surfaces and higher roughness. In the present case the feed per tooth is equal to 1 µm that is very near to the Minimum Uncut Chip Thickness (MUCT) that depends on the cutting-edge radius of the micro-mill and was determined by preliminary tests on the 200 µm micro-mill.

In Fig. 8, the amplitude parameters show that the peaks and valleys distributions of the machined surfaces are fairly comparable for both methods. The surfaces are distinguished by profiles with deleted peaks or deep scratches, as well as a leptokurtic surface (many high peaks and deep valleys). This shows that MM (Fig. 8a) and micro-EDM (Fig. 8b) both improve the surface quality without changing the texture.

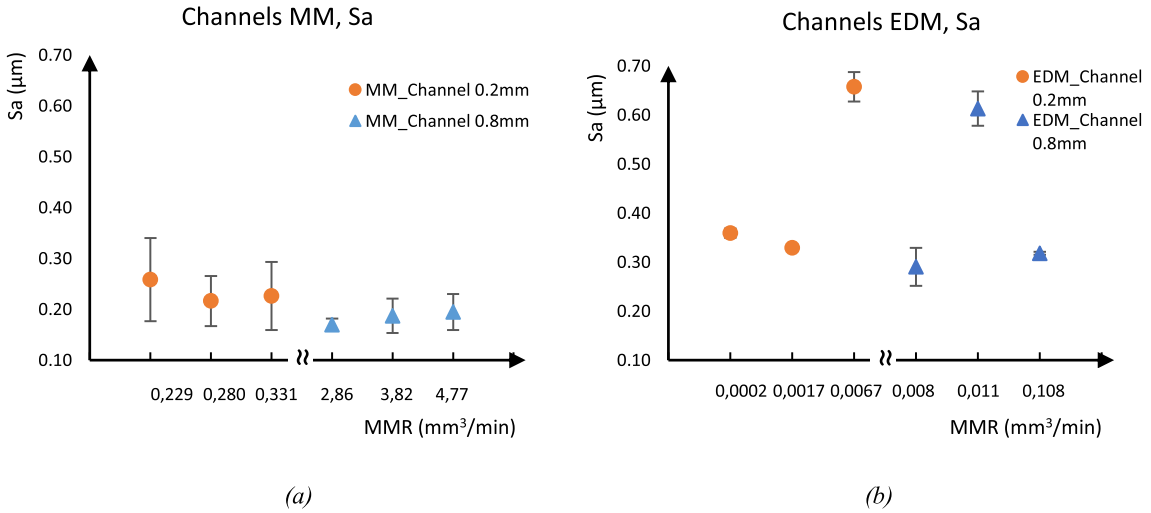

Fig. 7 Surface finishing on the bottom of the channel for MM (**a**) and micro-EDM (**b**)

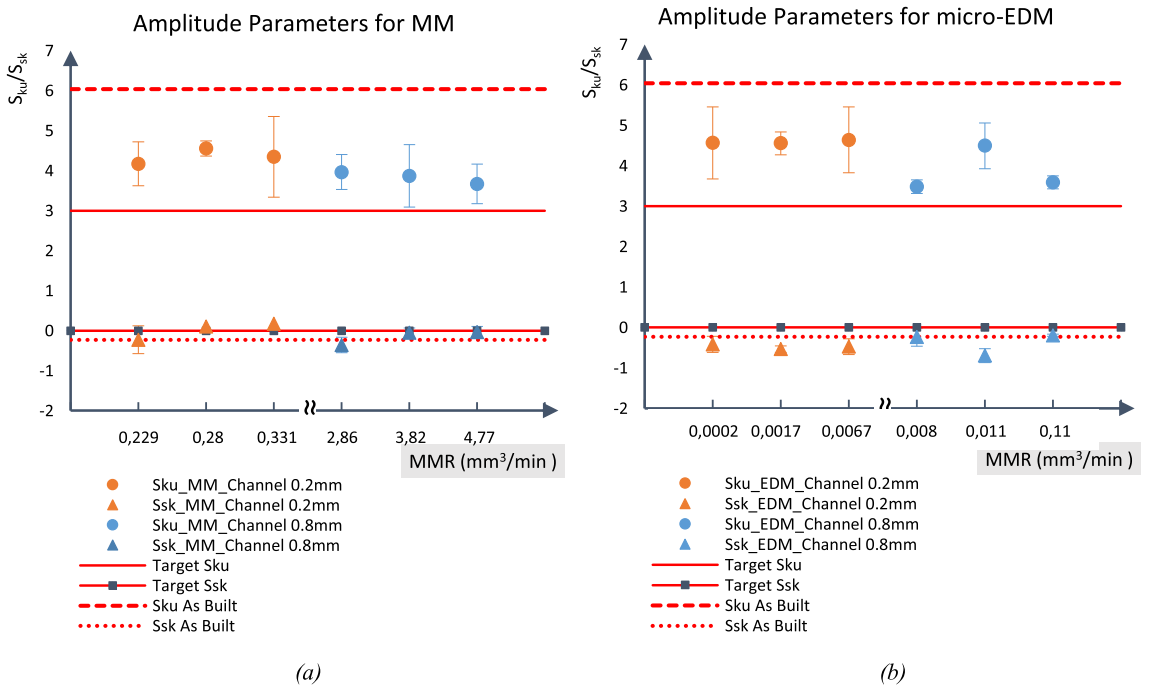

Fig. 8 Amplitude parameters on the bottom of the channel for MM (**a**) and micro-EDM (**b**)

Burrs and recast particles

A further characteristic of the examined processes is the machining markings represented by burrs for MM and recast particles for micro-EDM, which might be considered a defect or a limitation for the part's applicability. The predicted area's extension was approximated in both cases using the approaches described in the previous section. Both machining had an excess of material, as seen in Fig. 9. Micro-machining, in particular, produces large burr extension and high unpredictability, making it impossible to anticipate the defect (Fig. 9a). Micro-EDM, on the other hand, has low excess material on the surface and limited variability, demonstrating stability in this conditions (Fig. 9b).

Conclusion

The micro-machinability of additively made stainless steel was investigated in this research using MM and micro-EDM techniques. The parts were produced using a LPBF process using 17-4PH stainless steel. This research was aimed to

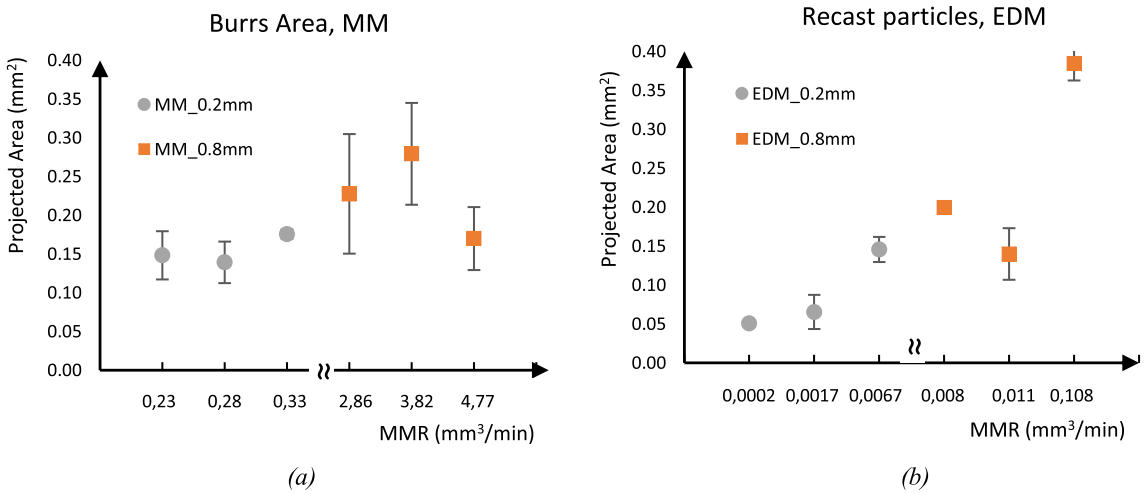

Fig. 9 Burrs extension on the side of the channels for MM (**a**) and recast particles area for micro-EDM (**b**)

investigate the outcomes on the surface quality and geometrical accuracy resulting from micro-Milling and micro-EDM processes on LPBF samples of the same material. Specifically, the novelty of this approach relies on the presence of specific features to realize: holes and channels with dimensions of 200 µm and 800 µm for both procedures. The holes and channels were produced on both as-built and pre-processed surfaces, and the results in terms of dimensional accuracy were related to the material removal rates and tool dimension. The size effects of each process were related to the features dimension highlighting the limits of each micro-machining technique. Moreover, the analysis of surface quality, burrs, and particle presence was performed in relation to the *MRR*, allowing a better comparison between traditional and non-traditional techniques.

Due to the following findings, the results of this study potentially go beyond the state of the art:

- The *MRR* achievable by micro-EDM are much lower then the *MRR* reachable by MM.
- The micro-EDM technique may be more suitable for drilling considering the stability of the process that assures good dimensional accuracy even on surfaces with high roughness (as-built samples).
- MM, despite the calibration of the tools with low run-out for high-precision machining, may be limited to pre-machined surfaces.
- MM drilling: The diameter increases as the *MRR* increases for Ø 800 µm holes due to the tool run-out effect, while the trend is opposite for Ø 200 µm holes. In this case, the spindle speed limits the cutting speed which results inadequate with the lowest *MRR*.
- Micro-EDM drilling: The diameter and circularity of the holes do not depend on the *MRR* or the wire size.
- Micro-drilling: The dimensional accuracy is better with MM while the shape quality is better with micro-EDM.
- Micro channels: The geometrical accuracy does not depend on the *MRR*. Both processes show high stability.
- MM allowed to achieve a better surface finish having a S_a lower than 0.3 µm regardless of the feature size or the process parameters. The surface roughness (S_a) increased for feed rates smaller than 1 µm/tooth, exhibiting a ploughing-dominated zone (Abeni et al., 2021a).
- Micro-EDM: the S_a values are higher reaching a maximum of 0.66 µm, due to the typical craters of this process.
- The surface quality is more related to the tool width (MM) and discharge levels (micro-EDM) than to the *MRR*.
- Micro-EDM process exhibits minimal excess material and offers a higher control on the presence of recast particles.
- MM technique may cause an excessive and not predictable extension of the burrs requiring deburring post-process. Optimizing cutting parameters can help to minimize burr formation.

These findings can be exploited for several fields of application, especially considering the necessity of machining post-processing following Powder Bed Fusion processes of metals for the production of functional, complex, and bespoke parts. Specifically, automotive and aerospace fields would benefit from more research about the post-production processes of 3D-printed metal parts since highly complex and micro-scale geometries are required with the necessity of standard procedures and series productions that machining can promote. Furthermore, the biomedical sector is massively working on bespoke and personalized parts leading to an expansion of 3D sample production but requiring both surface quality and geometrical accuracy that can highly influence the outcome of an implant in terms of revision requirements and patient quality of life. Finally,

design applications have recently more focused on modular parts and efficient assembly requirements and need further developments in post-processing for dimensional tolerance specifications.

For these reasons, future studies on 3D-printed metal machining results will help optimize the traditional and not-traditional process parameters for a broader range of materials and understand the potential of micro-machining on different types of parts. Further research is needed to reach the point where every 3D metal component can assure high surface finishing and accuracy without chemical post-processes that are nowadays used for processing complex micro-parts and often lead to poor surface quality and possible chemical residuals.

Moreover, LPBF process parameters, such as layer thickness and hatch spacing, will be studied in future studies, resulting in variable melt path width-to-height ratios. The effects of the anisotropic material structure on tool wear, process forces, burr development, and roughness described in this work will be confirmed by using these novel process parameters and applying heat treatments.

Acknowledgements Financed by the European Union—NextGenerationEU (National Sustainable Mobility Center CN00000023, Italian Ministry of University and Research Decree n. 1033-17/06/2022, Spoke 11-Innovative Materials & Lightweighting). The opinions expressed are those of the authors only and should not be considered as representative of the European Union or the European Commission's official position. Neither the European Union nor the European Commission can be held responsible for them. CUP D83C22000690001.

Author contributions AA, MQ, PSG contributed to the study conception and design. Material preparation, data collection and analysis were performed by AA and MQ. The first draft of the manuscript was written by AA, MQ and PSG and AA, MQ, PSG commented on previous versions of the manuscript. AA, MQ, PSG read and approved the final manuscript.

Funding Financed by Regione Lombardia (Italy), regional law no 9/2020, resolution no 3776/2020.

Data availability The data that support the findings of this study are not openly available due to reasons of sensitivity and are available from the corresponding author upon reasonable request. Data are located in controlled access data storage at the University of Brescia.

Declarations

Competing interest The authors have no relevant financial or non-financial interests to disclose.

References

Abeni, A., Ginestra, P. S., Attanasio, A. (2021). Micro-milling of selective laser melted stainless steel. In Selected topics in manufacturing. Lectures notes in mechanical engineering; Springer: Cham, pp. 1–12.

Abeni, A., Ginestra. P. S., Attanasio, A. (2022). Comparison between micro machining of additively manufactured and conventionally formed samples of Ti6Al4V alloy. In Selected topics in manufacturing. Lectures notes in mechanical engineering; Springer: Cham, pp. 91–106.

Abeni, A., Loda, D., Özel, T., & Attanasio, A. (2021b). Modeling of cutting force in micro-end-milling process with experimental validation on additive manufactured Nickel-based superalloy. *Procedia CIRP, 102*, 222–227.

Bai, Y., Zhao, C., Yang, J., Hong, R., Weng, C., & Wang, H. (2021). Microstructure and machinability of selective laser melted high-strength maraging steel with heat treatment. *Journal of Materials Processing Technology, 288*, 116906.

Balázs, B. Z., Geier, N., Takács, M., & Davim, J. P. (2021). A review on micro-milling: Recent advances and future trends. *International Journal of Advanced Manufacturing Technology, 112*(3), 655–684.

Bissacco, G., Hansen, H. N., & Slunsky, J. (2008). Modelling the cutting-edge radius size effect for force prediction in micro milling. *CIRP Annals-Manufacturing Technology, 57*, 113–116.

Cooke, S., Ahmadi, K., Willerth, S., & Herring, R. (2020). Metal additive manufacturing: Technology, metallurgy and modelling. *Journal of Manufacturing Processes, 57*, 978–1003.

D'Urso, G., Giardini, C., Lorenzi, S., Quarto, M., Sciti, D., & Silvestroni, L. (2020). Micro-EDM milling of zirconium carbide ceramics. *Precision Engineering, 65*, 156–163.

D'Urso, G., Giardini, C., & Quarto, M. (2018). Characterization of surfaces obtained by micro-EDM milling on steel and ceramic components. *International Journal of Advanced Manufacturing Technology, 97*, 2077–2085.

Franczyk, E., Machno, M., & Zębala, W. (2021). Investigation and optimization of the SLM and WEDM processes' parameters for the AlSi10Mg-sintered part. *Materials (basel), 14*(2), 410. https://doi.org/10.3390/ma14020410

Galati, M., Minetola, P., & Rizza, G. (2019). Surface roughness characterization and analysis of the electron beam melting (EBM) process. *Materials, 12*(13), 2211.

Gomes, M. C., dos Santos, A. G., de Oliveira, D., et al. (2022). Micro-machining of additively manufactured metals: A review. *International Journal of Advanced Manufacturing Technology, 118*, 2059–2078. https://doi.org/10.1007/s00170-021-08112-0

Greco, S., Kieren-Ehses, S., Kirsch, B., et al. (2021). Micro milling of additively manufactured AISI 316L: Impact of the layerwise microstructure on the process results. *International Journal of Advanced Manufacturing Technology, 112*, 361–373. https://doi.org/10.1007/s00170-020-06387-3

Hassanin, H., Modica, F., El-Sayed, M., Liu, J., & Essa, K. (2016). Manufacturing of Ti–6Al–4V micro-implantable parts using hybrid selective laser melting and micro-electrical discharge machining. *Advanced Engineering Materials*. https://doi.org/10.1002/adem.201600172

Ji, H., Gupta, M. K., Song, Q., Cai, W., Zheng, T., Zhao, Y., et al. (2021). Microstructure and machinability evaluation in micro milling of selective laser melted Inconel 718 alloy. *J Mater Res Technol, 14*, 348–362.

Karakılınç, U., Ergene, B., Yalçın, B., Aslantaş, K., & Erçetin, A. (2023). Comparative analysis of minimum chip thickness, surface quality and burr formation in micro-milling of wrought and selective laser melted Ti64. *Micromachines, 14*(6), 1160. https://doi.org/10.3390/mi14061160

Kasperovich, G., Haubrich, J., Gussone, J., & Requena, G. (2016). Correlation between porosity and processing parameters in TiAl6V4 produced by selective laser melting. *Materials and Design, 105*, 160–170.

Khaliq, W., Zhang, C., Jamil, M., & Khan, A. M. (2020). Tool wear, surface quality, and residual stresses analysis of micro-machined

additive manufactured Ti–6Al–4V under dry and MQL conditions. *Tribology International, 4*, 106408.

Korner C, Group F. (2016). Additive manufacturing of metallic components by selective electron beam melting: A review. *International Materials Reviews, 61*, 361–377.

Kumar, D., Singh, N., & Bajpai, V. (2020). Recent trends, opportunities and other aspects of micro-EDM for advanced manufacturing: A comprehensive review. *Journal of the Brazilian Society of Mechanical Sciences and Engineering, 42*(5), 221–247.

Le Coz, G., Fischer, M., Piquard, R., D'acunto, A., Laheurte, P., Dudzinski, D. (2017). Micro cutting of Ti-6Al-4V parts produced by SLM process. *Procedia CIRP, 58*, 228–232. https://doi.org/10.1016/j.procir.2017.03.326

Le Coz, G., Piquard, R., D'Acunto, A., Bouscaud, D., Fischer, M., & Laheurte, P. (2020). Precision turning analysis of Ti-6Al-4V skin produced by selective laser melting using a design of experiment approach. *International Journal of Advanced Manufacturing Technology, 110*, 1615–1625.

Liu, C., Yan, D., Tan, J., Mai, Z., Cai, Z., Dai, Y., et al. (2020). Development and experimental validation of a hybrid selective laser melting and CNC milling system. *Additive Manufacturing, 36*, 101550.

Nas, E., & Akıncıoğlu, S. (2019). Optimization of cryogenic treated nickel-based superalloy in terms of electro erosion processing performance. *Academic Platform Journal of Engineering and Science, 7*(1), 115–126.

Quarto, M., Bissacco, G., & D'Urso, G. (2019). Machinability and energy efficiency in micro-EDM milling of zirconium diboride reinforced with silicon carbide fibers. *Materials, 12*(23), 78.

Sahoo, P., Patra, K., Szalay, T., & Dyakonov, A. A. (2020). Determination of minimum uncut chip thickness and size effects in micro-milling of P-20 die steel using surface quality and process signal parameters. *International Journal of Advanced Manufacturing Technology, 106*(11), 4675–4691.

Shivanna, D. M., Kiran, M. B., & Kavitha, S. D. (2014). Evaluation of 3D surface roughness parameters of EDM components using vision system. *Procedia Materials Science, 5*, 2132–2141.

Tan, J. H. K., Sing, S. L., & Yeong, W. Y. (2020). Microstructure modelling for metallic additive manufacturing: A review. *Virtual Phys Prototyp, 15*(1), 87–105.

Varghese, V., & Mujumdar, S. (2021). Micromilling-induced surface integrity of porous additive manufactured Ti6Al4V alloy. *Procedia Manuf, 53*, 387–394.